Available online at www.sciencedirect.com
ScienceDirect
Journal of the European Ceramic Society 29 (2009) 1419–1425
www.elsevier.com/locate/jeurceramsoc

Temperature distribution for electrically conductive and non-conductive materials during Field Assisted Sintering (FAST)

Jan Räthel *, Mathias Herrmann, Wieland Beckert

Fraunhofer Institute for Ceramic Technologies and Systems, Winterbergstrasse 28, D-01277 Dresden, Germany

Received 30 April 2008; received in revised form 12 September 2008; accepted 13 September 2008
Available online 7 November 2008

Abstract

During Field Assisted Sintering Technology (FAST) the temperature differences at two different positions were investigated using two pyrometers, an internal and an external one. Two substances, an electrically conductive (tungsten carbide) and a non-conductive material (96 wt.% silicon nitride with 2 wt.% alumina and yttria) were used to monitor the temperature differences between both pyrometers during heating, sintering shrinkage and dwell time by varying die geometry and heating rate. It was shown that the temperature distribution is strongly influenced by the electrical conductivity of the material as well as by tool design and setup. The alpha–beta transformation of silicon nitride was analyzed to predict the radial temperature distribution within the sample. For comparison and for visualization a dynamical FE model including piston movement for simulating sintering shrinkage was introduced. With this, a complete time dependent FAST run could be simulated. The modeled differences in temperature distribution are in good agreement with real temperature measurements as well as phase analyses.

Keywords: Field Assisted Sintering; Carbides; Si_3N_4; Refractories; Electrical properties

1. Introduction

Field Assisted Sintering Technology (FAST) can be described as a combination of a uniaxial pressing process and a direct passing of electric DC current through the graphite tool and the specimen, if it is electrically conductive. The production of Joule heat within tool and material enables high heating rates. So, the densification of various materials with higher heating rates and shorter dwell times becomes possible. That is one of the reasons, why more and more attention is paid to the process of Field Assisted Sintering Technology. The number of articles dealing with this kind of sintering method is rising. In 2007, more than 470 papers were published. The research includes all fields of materials starting from intermetallics,[1–2] thermoelectrics,[3–4] ceramics and composites,[5–7] functional graded materials[8–9] and hard metals.[10–11] There are just a few articles existing who mainly deal with investigations on the process itself. Temperature measurements at more than one position can be rarely found[12–13] but these investigations are fundamental to estimate the real temperature distribution within the sample. They are the preconditions for the preparation of homogeneous materials and for the comparison of the results achieved at different FAST/SPS devices. Vanmeensel et al.[12] consolidated an electrically conductive powder close to percolation threshold. The material switches from electrical non-conducting to conductive as the volume of porosity disappeared. It was observed that the temperature measured on the outside of the die reduces with decreasing resistivity of the material.

Several authors have brought forward proof that measured temperature is strongly influenced by electrical and thermal conductivity and the dimension of the tool setup[14–15] as well as the powder that is consolidated.[12,14] A systematic measurement of the temperature at different positions (inside, outside of the die) for different tool designs and materials gives the possibility to evaluate the temperature distribution during FAST/SPS comparing these results by FE modeling.

Numerical simulation is a promising tool being able to model different systems or problems described by mathematical equations. Static FE simulations were introduced to the process of Field Assisted Sintering Technology.[16–18] A FE model can help to understand the temperature distribution inside the FAST/SPS tool for different sintered materials, tool materials and tool

* Corresponding author. Tel.: +49 351 2553967; fax: +49 351 2553600.
E-mail addresses: jan.raethel@ikts.fraunhofer.de, Jan.raethel@fetene.de (J. Räthel).

0955-2219/$ – see front matter © 2008 Elsevier Ltd. All rights reserved.
doi:10.1016/j.jeurceramsoc.2008.09.015

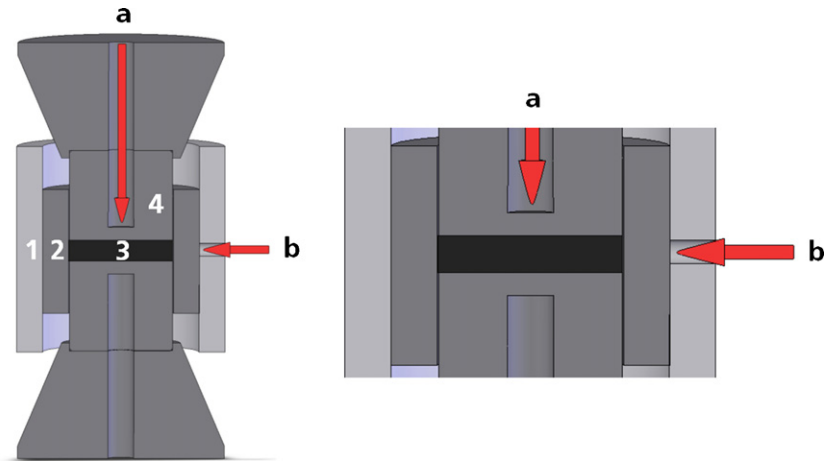

Fig. 1. Experimental setup (1, graphite felt; 2, die; 3, specimen; 4, punch) with two temperature measuring positions (a, inner temperature; b, outer temperature).

setups. So, the estimations done have to be controlled by experimental procedures and measurements.[12–13] Most FE modeling is related to symmetrical tool setups, but also non-cylindrical geometry FE models are introduced.[18] Because of the different setups, tool sizes and materials as well as temperature measuring position used, comparisons between the two major suppliers for FAST/SPS devices (SPS Syntex Inc., Japan; FCT Systeme GmbH Germany) are difficult. The application of graphite foil as a connector between different parts of the tool setup is one of the biggest challenges, because foil properties change depending on temperature and pressure appliance.[10]

The aim of this paper is to evaluate the temperature distribution during FAST/SPS for a conductive (tungsten carbide) and a non-conductive material (silicon nitride) by varying materials parameters as well as measuring the temperature at different positions. The results are compared with the calculated ones.

2. Experimental setup and starting material

The standard experimental setup is shown in Fig. 1. Two temperature-measuring positions were chosen, the internal pyrometer position (a) and an external one (b) measuring the temperature on the surface of the die. Temperature measurement at the internal pyrometer was used to adjust current and voltage for controlling heating rate and temperature during the entire FAST/SPS run. The graphite tool setup (SGL Carbon Group, R7710), horizontal and vertical layers of graphite foil (SGL Carbon Group) and a graphite felt as thermal insulation was used. For the external measuring device a hole with a diameter of 7 mm was cut into the graphite felt. If there are no other remarks in this paper, the tool was heated using graphite felt insulation.

Commercially available pure tungsten carbide (99.9% purity; $d_{50} = 0.8\ \mu m$) was used as conducting powder. Silicon nitride (Silzot HQ; 98% purity; $d_{50} < 2.5\ \mu m$; SKW GmbH; Germany) was used as a non-conductive powder with sintering additives of 2 wt.% yttria (99.99% purity; $d_{50} < 2\ \mu m$; Treibacher Industrie AG; Austria) and 2 wt.% alumina (AKP50; 99.99% purity; Sumitomo Chemical Company, Lim.; Japan). After ball milling the powder was granulated.

The transformation of alpha and beta-silicon nitride is mainly influenced by temperature and time as well as dissolution diffusion and a precipitation mechanism.[5–6] So, the change in alpha/beta ratio as a function of time and temperature can be used to estimate real temperature distribution as a function of distance from the specimen center. The alpha/beta ratio was calculated on the basis of XRD measurements (Cu-K-alpha) and quantitative analysis using the Rietveld method (Autoquan, GE Inspection Technologies).

The amount of powder was weighed to obtain fully dense samples with a height of 5 mm to minimize the influence of sample height on temperature distribution. Experiments were performed by varying sample diameter, heating rate and die thickness (Table 1). The densities of the samples are given in Table 2.

The FE model was developed by using FlexPDE© as a multiphysics finite elements solution environment, taking advantage of the codes flexibility allowing the user very convenient and efficient adaptions in the implementation of a physical problem.

The model is based on the coupled balance equations of thermal energy and electrical energy transport and takes advantage of the cylindrical geometry by using an axisymmetric formulation. In addition to the conductive heat transport in the material

Table 1
Parameter setup used for FAST consolidation.

Material	Conditions				Die	
	Heating rate (K/min)	Pressure (MPa)	Temperature (°C)	Time (min)	Diameter (mm)	Thickness (mm)
Si_3N_4	100; 50	50	1750	5	30; 40	10; 15
WC	100; 50	50	2000	5	30; 40; 60	10; 15

Table 2
Measured and modeled temperature and temperature differences between external and internal pyrometer for a 40 mm tool during hold time.

Material	Measured		Modeled		
	a (°C)	b (°C)	a (°C)	b (°C)	ΔT_{sample} (°C)
Si_3N_4	1750	1886	1750	1800	60
Si_3N_4	1750	1787	1750	1700	40
WC	2000	1960	2000	1920	40
WC	2000	1884	2000	1830	60

a convective heat transport in the moving parts of the sample has to be considered. The model geometry includes the full sample, complete graphite tool and part of the water-cooled metal pistons in order to homogenize the local details of piston cooling. Since for temperatures above 800 °C radiative heat transfer from the sample surface becomes dominant, a combined free convection and surface to ambient thermal radiation heat transfer between sample surface, tool and the water-cooled metal pistons was implemented as an external boundary condition. Due to the thermal radiation, the term of electrical nonlinear Joule heat production and the considered temperature dependence of the material properties the model has a nonlinear character. The transient formulation of the model allows to account for the thermal lag of the system and to analyze its dynamic behavior. There are two aspects, which distinguish the model from other model analyses known to the authors:

- the change of the geometry due to the movement of the pistons and the compaction can be taken into account by help of a moving mesh approach which works by mapping a (prescribed) transformation of the geometry on a fixed mesh,
- the implementation of a simple temperature control run by help of a scalar variable that allows the emulation of a temperature controlled loading process instead of a simply prescribed electrical voltage or current ramp.

The model enables to calculate a completely parameterized tool setup and to easily change the listed materials properties within a database. Therefore, it is possible to simulate a complete time dependent FAST/SPS run, including piston movement for the simulation of sintering shrinkage. FE modeling was used to predict the temperature distribution during Field Assisted Sintering and to compare the results with the measured temperatures. The material properties (electrical resistivity, thermal conductivity) as a function of temperature were taken from the supplier of the graphite.

3. Results

Fig. 2 shows power consumption, piston travel and temperature of the internal and external pyrometer for silicon nitride and tungsten carbide being consolidated in a tool with a diameter of 40 mm using a thin die. Power consumption shows no difference between the sintering of an electrically conductive or non-conductive material. The piston travel varies because tungsten carbide precompaction is lower as the used silicon nitride composite material and sintering starts at different temperatures (silicon nitride 1100 °C; tungsten carbide 1450 °C). A pressure of 50 MPa was applied between 900 and 1000 °C. Even if sintering shrinkage is different, the power consumption during heating ramp is nearly the same for both materials. The temperatures measured at position (a) and (b) in Fig. 1 during heating ramp show a higher temperature on the outside of the die for silicon nitride (100 to 140 °C) and for tungsten carbide a temperature similar to that of the internal pyrometer (40 to 10 °C). For all other tool sizes and setups,

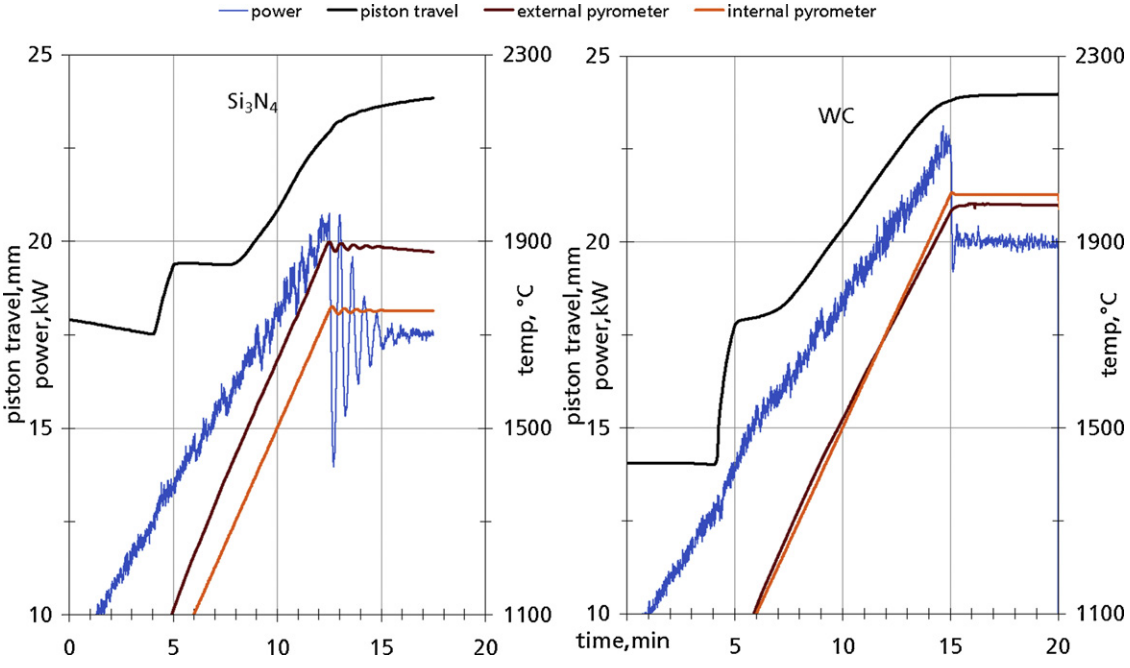

Fig. 2. Power, piston travel, and temperature at the two measuring points for the Si_3N_4 densified at 1750 °C (a) and WC 2000 °C (b).

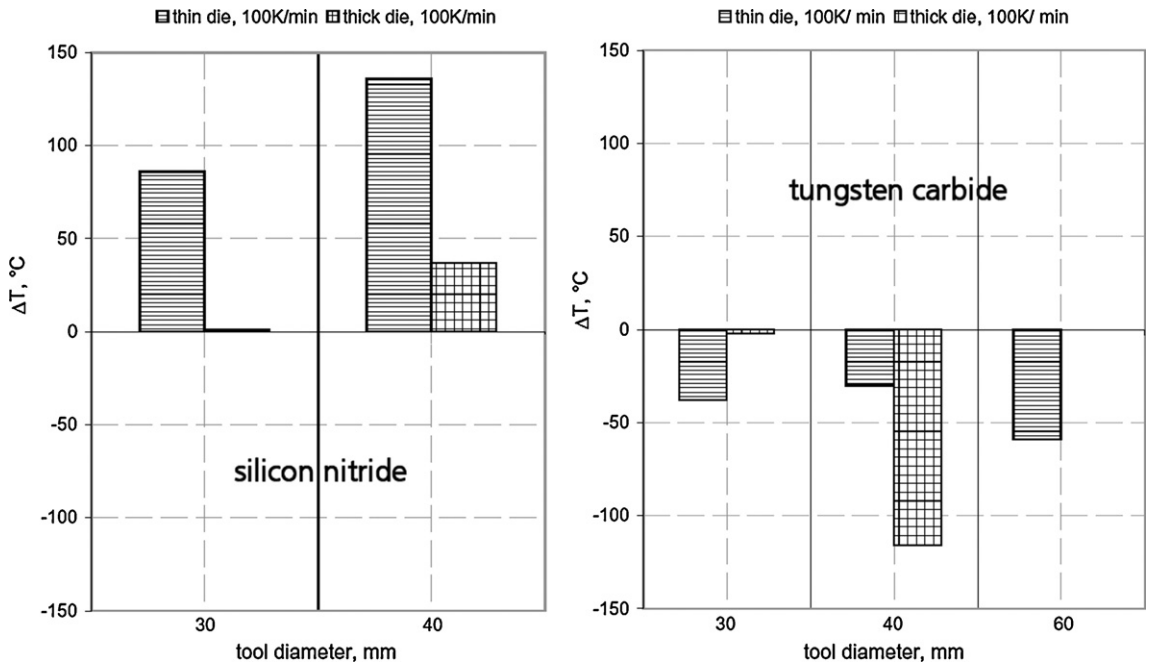

Fig. 3. Temperature difference ΔT between external and internal controlling pyrometer during dwell time.

Fig. 3 illustrates temperature differences between the external and internal pyrometer during dwell time only.

During densification of the silicon nitride powder, in any case a higher temperature on the outside of the die was measured as compared to the internal pyrometer (Fig. 3). Using a tool with a wall thickness of 10 mm (thin die), the temperature difference during dwell time is higher than using a die with a wall thickness of 15 mm (thick die). So, the temperature difference increases with increasing tool diameter.

During densification of tungsten carbide, the temperature on the outside of the die was lower than the temperature measured at the inner pyrometer under all used conditions. Temperature difference rises with increasing tool diameter (Fig. 3). If the densification of the tungsten carbide powder was carried out without a graphite felt, the temperatures on the outside of the die only reached 1650 °C during dwell time at 2000 °C. If the direct electrical current flow through the tungsten carbide specimen is disabled due to a horizontal graphite foil with a boron nitride layer of 0.5 mm thickness the temperature on the outside of the die reaches higher values. The temperature difference between internal and external pyrometer (Fig. 1) was reduced from 40 °C for the standard setup of 25 °C for the BN layered tool setup only.

Fig. 4 shows the current density distribution (A/m^2) during isothermal heating for both materials (D40 mm tool). The current distribution gives an idea of the Joule heat generated at the different positions without having any heat losses for the same tool setup, and is mainly attributed to the consolidated material as well as the geometric details of the tool. For silicon nitride, no current passes through the sintering material but in case of tungsten carbide, the current density within the material is half of the current density in the die, indicating also a heating of the sample itself. During the densification of the WC powder, a maximum of the current density is located in the punches, indicating that an intensive heating takes place. This leads to different temperature distributions for both materials within the tool and the specimen, as depicted in Fig. 5.

Modeled data are given for the tool diameter of 40 mm only. The modeled temperature distribution for silicon nitride reaches values of 1750 °C at position a (Fig. 1) for both die sizes, but the temperature of the external pyrometer is different. 1800 °C for the thin die and 1700 °C for the thick die were calculated and compared to the measured values of 1886 °C for the thin and 1787 °C for the thick die (Table 2). The measured values are higher than the simulated ones and the difference in temperature is about 80 to 90 °C. The temperature gradient within the sample volume can be decreased by increasing the die thick-

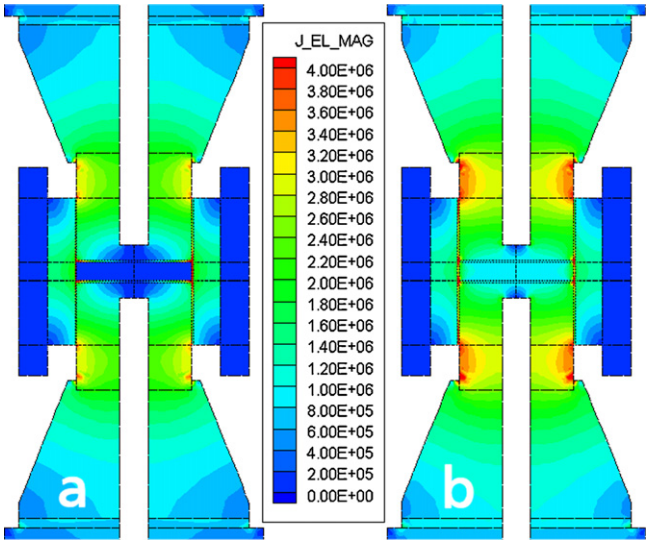

Fig. 4. FE modeled current density distribution for D40 mm tool with thin die during dwell time for tungsten carbide (a) and silicon nitride powder (b).

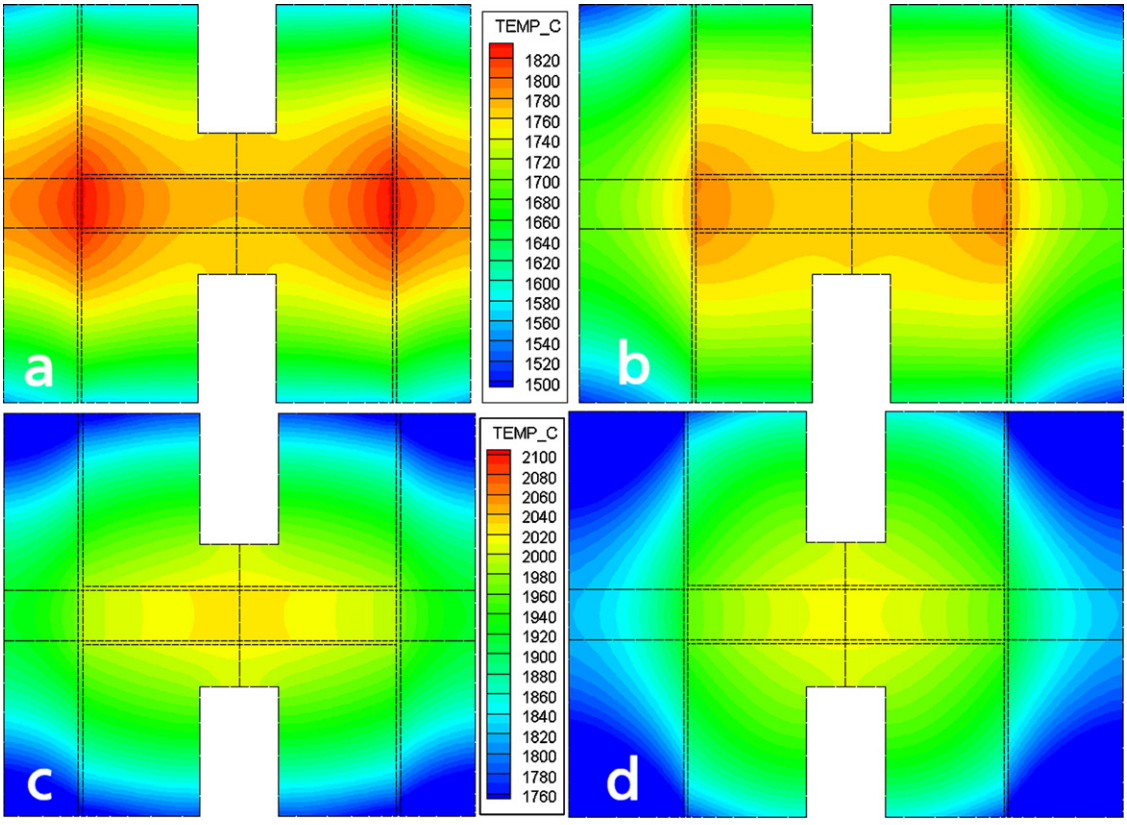

Fig. 5. FE modeled temperature distribution for D40 mm tool during dwell time for silicon nitride, (a) Thin die, (b) thick die and tungsten carbide, (c) thin die, and (d) thick die.

ness. So, an overheating of the sample close to the die can also be minimized.

For tungsten carbide, a temperature of 2000 °C was measured for both die sizes at position a (Fig. 1). At the external pyrometer position temperatures of 1960 °C (thin die) and 1884 °C (thick die) were measured and compared to the calculated temperatures of 1920 and 1827 °C. All temperatures of the external pyrometer are lower than those measured at the internal pyrometer position. The difference in temperature for tungsten carbide samples is a little bit lower than for silicon nitride samples and is about 40 to 55 °C. The temperature gradient within the sample volume can be decreased by decreasing the die thickness. In consequence, to minimize temperature gradients the die has to be reduced to the lowest thickness, which is still mechanically stable.

Because of the low amount of oxide additives, the silicon nitride samples obtained were not dense (Table 3). In any case, the samples being consolidated using a thin die showed higher densities than those being consolidated using a thick die independent of tool diameter. The ratios of alpha/beta-Si_3N_4 observed at different distances from the center clearly indicate that a temperature distribution is indirectly observable and is strongly influenced by die thickness (Fig. 6). Higher temperatures at same exposure time will decrease the alpha-silicon nitride content. The alpha/beta-Si_3N_4 ratio observed at different distances from the center show that a less uniform temperature distribution is achieved with a thinner die, which is in good agreement with the modeled data (Fig. 5).

All tungsten carbide samples were dense (100% of theoretical density). Measurements of hardness as a function of the radius for all samples and all diameters showed no reaction to the measured and calculated temperature gradients observed.

4. Discussion

Temperature distribution during Field Assisted Sintering is strongly dependent on tool size, heating rate and properties of the consolidated material. If a non-conductive specimen is consolidated, most of the Joule heat will be produced within the

Table 3
Densities of the samples as a function of tool size.

Tool size (mm)	Density of silicon nitride (g/cm^3)		Density of tungsten carbide (g/cm^3)	
	Thin die	Thick die	Thin die	Thick die
30	3.07	2.92	15.75	15.74
40	3.04	2.99	15.77	15.73
60	–	–	15.78	–

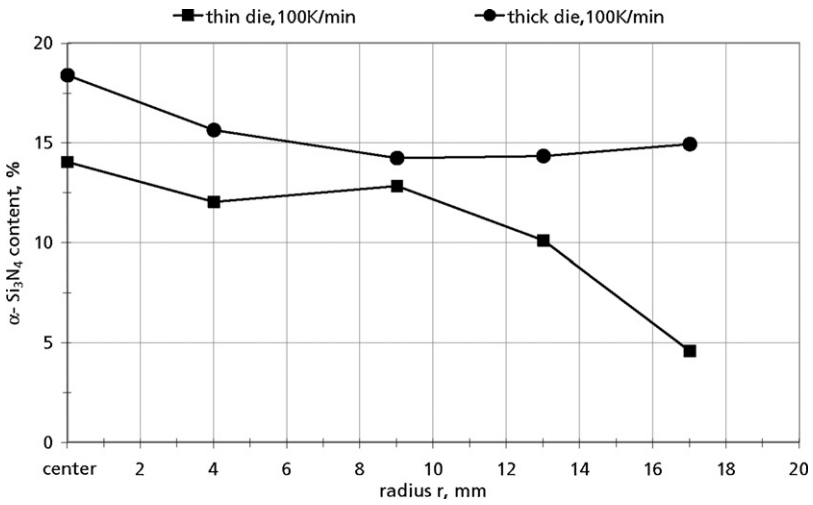

Fig. 6. α-silicon nitride content as a function of distance from sample centre (samples with a diameter of 40 mm at a heating rate of 100 K/min.

three-phase area of piston, graphite foil and die. So, temperature distribution is mainly influenced by the die thickness and tool diameter. Joule heat is produced within the graphite volume and has to be transported to the whole sample volume. If the specimen diameter increases, the production of heat has also to be increased. So, overheating close to the die will be observed for small dies. In addition, the thermal conductivity of traditional sintered silicon nitride at temperatures of about 1750 °C is low (approximately 10 W/m K [5]) in comparison to that of tungsten carbide at 2000 °C (approximately 30 W/m K).[19] Therefore, tool design is one possibility to minimize temperature gradients and enhances the benefit of FAST sintering method.

Modeled and measured temperature data are in good agreement and show the same tendency in temperature change. The differences in temperature between modeled and measured data are influenced by the exact positioning of both pyrometers (especially for the external one, which moves due to sintering shrinkage). The radiation losses at the external pyrometer position (hole in thermal insulation) were not taken into account for the FE simulation. The FE model is idealized, possesses perfect contacts and therefore realizes perfect heat transport (not affected by pressure-dependent heat flow) between each part of the tool. In literature no information can be found on temperature-dependent material properties, approximations were used for higher temperatures, because the sample properties are strongly connected to the microstructure obtained by FAST, especially thermal and electrically properties. Taking into account all these problems and difficulties the achieved results of the FE model can be validated by the used two-point temperature measuring technique. The differences between measured and modeled data show also the complexity of this task. The achieved results of temperature distribution within the sample volume can be used to construct tools leading to minimized temperature gradients.

Phase analysis of the alpha-silicon nitride content indicates that the radial temperature distribution is strongly influenced by tool geometry, which is in good agreement with FE modeling. A thin die leads to a bigger temperature difference between center and outer area of a non-conductive sample, because the current passes the die close to the specimen volume. These results also show clear evidences that temperature differences during compaction of conductive and non-conductive sample are closely related to electrical and thermal conductivity.

Tungsten carbide shows a more homogeneous temperature distribution (less overheating then for silicon nitride) within the sample volume using a thinner die. The temperature on the outside of the die decreases if the die thickness will be increased, because also the sample itself produces Joule heat by passing electric current through it. For the production of electrically conductive samples the thinnest applicable die thickness should be used.

The use of a shielding insulation is essential, because of energy losses at high temperatures, which lead to a more explicit temperature distribution within the sample volume and tool. This is mainly induced by radiation losses, which strongly increase with the temperature (Stefan–Boltzman law). In most investigations in the past, a shielding insulation was not used and "low temperature sintering" results were achieved only in correspondence with wrong temperature measurements. Even if a shielding insulation was used the temperatures achieved at the external pyrometer led to measurements that differed much more from the real sample temperature (for example D40 mm tool thick die, tungsten carbide, $\Delta T \sim 170$ °C) than the measuring temperature at the internal pyrometer (in each case at ~10 to 20 °C). A description of the used tool geometry is essential being able to compare temperature measuring results achieved at different FAST/SPS devices.

5. Conclusion

- Temperature measurements during Field Assisted Sintering strongly depend on the positioning of temperature measuring devices, influenced by different tool setups and dimensions, which lead to different heating zones. Because of this, the sample temperature strongly depends on these problems and their intrinsic properties.

- Temperature distribution during Field Assisted Sintering is influenced by the tool geometry (die thickness and tool diameter) as well as the sintered material (electrically conductive or non-conductive material) and shielding insulation.
- The sintering of an electrically non-conductive material produces a higher temperature on the outside of the die as compared to a conductive sample.
- The alpha/beta ratio of silicon nitride compositions can be used to monitor the real temperature distribution during the FAST process.
- FE modeling is a powerful tool that enables the understanding of temperature distribution by changing tool geometry and size and can be validated by temperature measurements.

References

1. Schmidt, J., Weissgaerber, T., Schubert, T. and Kieback, B., Spark plasma sintering of intermetallics and metal matrix composites. *Advances in Powder Metallurgy & Particulate Materials*, 2006. pp. S9/85–S9/94.
2. Bernard, F. *et al.*, Dense nanostructured materials obtained by spark plasma sintering and field activated pressure assisted synthesis starting from mechanically activated powder mixtures. *Science of Sintering*, 2004, **36**(3), S155–S164.
3. Kim, S. S., Yin, F. and Kagawa, Y., Thermoelectricity for crystallographic anisotropy controlled Bi-Te based alloys and p–n modules. *Journal of Alloys and Compounds*, 2006, **419**(1–2), S306–S311.
4. Noda, Y., Plasma activated sintering of PbTe thermoelectric materials. *unknown*, 2006, **33**, S30–S33.
5. Petzow, G. and Herrmann, M., Silicon nitride ceramics. In *Structure and Bonding*, *vol. 102*. Springer Verlag, Berlin, Heidelberg, 2002, pp. 47–167.
6. Shen, Z., Zhe, Z., Peng, H. and Nygren, M., Formation of though interlocking and interlocking microstructures in silicon nitride ceramics by dynamic ripening. *Nature*, 2002, **417**, S266–S269.
7. Herrmann, M., Schulz, I., Bales, A., Sempf, K. and Hoehn, S., "Snow flake" structures in silicon nitride ceramics—reasons for large scale optical inhomogeneities. *Journal of the European Ceramic Society*, 2008, **28**(5), S1049–S1056.
8. Noguchi, T., Takahashi, K. and Masuda, T., Trial manufacture of functionally graded Si–Ge thermoelectric material. In *Functionally graded materials 1996, proceedings of the international symposium on functionally graded materials, 4th*, 1997, pp. 593–598.
9. Orihashi, M. *et al.*, Preparation and evaluation of PbTe-FGM by joining melt-grown materials. In *International conference on thermoelectrics, 16th*, 1997, pp. 379–381.
10. Vanmeensel, K., Laptev, A., Hennicke, J., Bourgeois, L., Vleugels, J. and Van den Biest, O., Finite element simulation of field assisted sintering of WC-Co based composites. *Internationales Plansee Seminar*, 2005, **16**, S266–S282.
11. Vanmeensel, K., Laptev, A., Hennicke, J., Vleugels, J. and Van der Biest, O., Modeling of the temperature distribution during field assisted sintering. *Acta Materialia*, 2005, **53**(16), S4379–S4388.
12. Vanmeensel, K., Laptev, A., Van der Biest, O. and Vleugels, J., Field assisted sintering of electro-conductive ZrO_2-based composites. *Journal of the European Ceramic Society*, 2006, **27**(2–3), S979–S985.
13. Wang, Y., Fu, Z., and Zhang, Q., SPS temperature distribution of different conductivity materials. In *Key engineering materials*, pp. 224–226; High-performance ceramics 2001, 2002, pp. 717–720.
14. Zhang, J., Zavaliangos, A. and Groza, J., The effect of specimen conductivity on current and temperature distribution in field activated sintering. In *Proceedings of the international conference. Part 4. Modeling. Volume: Advances in powder metallurgy & particulate materials*, 2003, pp. 89–99.
15. McWilliams, B., and Zavaliangos, A., Temperature distribution and efficiency considerations for field activated sintering (FAST). In *Sintering 2005*, vol. **2e2**, 2005, pp. 126–129.
16. Chang, F. C., Fessler, R. R., Merkle, B. D., Borton, J. M. and Goldberger, W. M., Computer modeling of temperature prediction for electroconsolidation. In *Proceedings of powder metallurgy alloys and particulate materials for industrial applications*, 2000, pp. 145–156.
17. Anselmi-Tamburini, U., Gennari, S., Garay, J. E. and Munir, Z. A., Fundamental investigations on the spark plasma sintering/synthesis process. II: Modeling of current and temperature distributions. *Materials Science & Engineering, A: Structural Materials: Properties, Microstructure and Processing A*, 2005, **394**(1–2), 139–148.
18. McWilliams, B., Zavaliangos, A., Cho, K. C. and Dowding, R. J., The modeling of electric current assisted sintering to produce bulk nanocrystalline tungsten. *Journal of the Minerals, Metals and Materials Society*, 2006, **58**(4), S67–S71.
19. Weimer, A. W., *Carbide, nitride and boride materials synthesis and processing*. Chapman & Hall, 1997.